BULLETIN OF THE POLISH ACADEMY OF SCIENCES
TECHNICAL SCIENCES, Vol. 72(5), 2024, Article number: e150202
DOI: 10.24425/bpasts.2024.150202

Application of continuous wavelet transform and convolutional neural networks in fault diagnosis of PMSM stator windings

Przemysław PIETRZAK and Marcin WOLKIEWICZ*

Wrocław University of Science and Technology, Department of Electrical Machines, Drives and Measurements, Wybrzeże Wyspiańskiego 27, 50-370 Wrocław, Poland

Abstract. Efficiency, reliability, and durability play a key role in modern drive systems in line with the Industry 4.0 paradigm and the sustainability trend. To ensure this, highly efficient motors and appropriate systems must be deployed to monitor their condition and diagnose faults during the operation. For these reasons, in recent years, research has been increasingly focused on developing new methods for fault diagnosis of permanent magnet synchronous motors (PMSMs). This paper proposes a novel hybrid method for the automatic detection and classification of PMSM stator winding faults based on combining the continuous wavelet transform (CWT) analysis of the negative sequence component of the stator phase currents with a convolutional neural network (CNN). CWT scalogram images are used as the inputs of the CNN-based interturn short circuits fault classifier model. Experimental tests were conducted to verify the effectiveness of the proposed approach under various motor operating conditions and at an incipient stage of fault propagation. In addition, the effects of the input image format, CNN structure, and training process parameters on model accuracy and classification effectiveness were investigated. The results of the experimental tests confirmed the high effectiveness of fault detection (99.4%) and classification (97.5%), as well as other important advantages of the developed method.

Keywords: fault diagnosis; interturn short circuits; continuous wavelet transform; convolutional neural networks; permanent magnet synchronous motor.

1. INTRODUCTION

Significant advantages such as high efficiency, wide speed control range, high reliability, and power density have made permanent magnet synchronous motors (PMSMs) popular in recent years [1]. They are increasingly used in a wide variety of industries, such as aerospace, automotive, robotics, HVAC/R and others [2]. However, PMSMs, despite their high reliability, are subject to various types of damage, including mechanical, magnetic, and electrical faults. Electrical faults are primarily short circuits in the stator winding, which are among the most common, and most destructive, faults of PMSMs [3]. Depending on the type, a distinction can be made between interturn short circuits (ITSCs), short circuits between coils in a single phase, phase-to-phase short circuits, and ground faults. Most often, a stator winding fault begins with ITSCs and then spreads rapidly from a single coil to subsequent coils, eventually leading to a phase-to-phase or phase-to-ground fault [4].

A short circuit usually occurs due to stator winding insulation damage caused by excessive mechanical, thermal, and electrical stresses that motors are subjected to during operation, often under harsh environmental conditions. Other factors that can contribute to faster degradation of a stator winding insulation and consequent short-circuiting include high dv/dt of the inverters supplying the motors, operation under load conditions exceeding the rated values, field weakening, and chemicals that may accelerate insulation aging [5].

ITSC causes high amplitude current flow in a shorted circuit, which leads to local excessive overheating of the stator winding, which in turn can lead to critical damage to the motor and the need to take it out of service. To avoid unexpected downtime in the processes in which these motors are used, as a result of the need to interrupt their operation, the condition of the stator winding should be continuously monitored, and its damage detected and classified as early as possible [6]. Early detection of a fault can enable proper scheduling of motor overhaul, which will translate into reduced repair costs, shorter delays, and lower production losses. In addition, it is extremely important for environmental concerns and sustainability, as it reduces the generation of additional waste.

Considering the above-mentioned risks arising from the lack of implementation of diagnostic methods, as well as the growing popularity of PMSMs, diagnostics of their faults seems to be essential. It has been of great interest both to university researchers and to industry in recent years. To meet these requirements, the development of such methods forces research into the possibility of using the latest technologies and innovative solutions. Appropriate selection and application of signal processing algorithms and artificial intelligence (AI) techniques make it possible to develop fully automated systems that allow real-time monitoring of motor conditions.

*e-mail: marcin.wolkiewicz@pwr.edu.pl

Manuscript submitted 2024-02-26, revised 2024-03-18, initially accepted for publication 2024-04-08, published in September 2024.

Over the years, many fault diagnosis methods have been developed for AC motors, including high-efficiency PMSMs [7–9]. These methods are based on diagnostic signals that carry information about the condition of the motor, such as stator phase current [10], axial flux [11], vibration [12], or signals from the control structure [13]. Among these signals, the most commonly used is the stator phase current.

To extract the fault symptoms from these diagnostic signals, signal processing algorithms are used. Among the most basic, and highly effective, is the spectral analysis of the signal using the fast Fourier transform (FFT) [14]. Advanced methods implementing frequency domain analysis used in PMSM fault diagnosis include higher order transforms (HOTs). One of the most popular and effective fault diagnosis tasks HOT is the bispectrum transform [15]. However, these methods also have limitations, such as the lack of information about the time of occurrence of a given component, and thus the ability to determine the timing of early fault symptoms.

Mathematical apparatuses that implement time-frequency domain analysis, such as the Hilbert-Huang transform [16], the short-time Fourier transform (STFT) [17], and the continuous wavelet transform (CWT) [18], are devoid of these disadvantages. In fault diagnosis, the effectiveness of CWT analysis has been verified mainly for fault diagnosis of induction motors [19]. However, despite the many advantages of this method, it was not extensively studied in the past for its applicability to the detection of PMSM stator winding faults at an incipient stage of fault development - as early as the short-circuiting of single turns to avoid fault propagation, and over a wide range of motor operating conditions.

The above methods can be used to extract symptoms of PMSM stator winding faults. To fully automate the process of monitoring and detecting stator winding damage, it is necessary to use a decision-making block that will generate information about the condition of the motor based on the extracted symptoms. In recent years, to minimize the role of the human expert, the process of automating this task has been implemented using AI techniques, such as machine learning (ML) algorithms [20] and artificial neural networks (ANNs) [21]. Proper selection and application of signal processing algorithms and the latest advances in AI make it possible to develop fully automated systems that allow real-time monitoring of machine operation. Among ANNs, research in recent years has focused most attention on deep neural networks, especially convolutional neural networks (CNNs). In the case of CNNs, it is possible to rely on raw diagnostic signals, omitting the signal processing stage, and achieving noticeably short detection times and high effectiveness, which has been studied and described in the literature [22]. However, this requires a CNN model with a more advanced structure and a longer training time, which can be reduced using advanced mathematical apparatuses-based signal preprocessing [15]. Combining the signal preprocessing stage with CNNs, whose main application is image recognition, using mathematical apparatuses whose result can be represented in the form of an image, can make it possible to achieve high effectiveness while reducing the network structure and the difficulty of the training process. Such solutions have so far been verified mainly for fault diagnosis of induction motors [23].

Nowadays, there is also a visible trend to apply advanced finite element method-based models of PMSMs with the ability to simulate several types of faults to generate their symptoms (features) that can be used for AI-based model training. This technique is one type of a rapidly developing approach called transfer learning (TF). In this type of TF, diagnostic methods are developed based on features preserved in diagnostic signals generated from the mathematical models of the motors. From these, datasets used to train AI-based fault detector models are prepared. The fault detector models, in turn, can be applied to real objects. Examples of such solutions for PMSM fault diagnosis are presented in [24–26]. However, model-based detection methods require extremely high computational power and a fully accurate representation of machine parameters, which can be difficult to determine precisely under real-world conditions.

This paper proposes a novel hybrid method for the automatic detection and classification of PMSM stator winding faults based on combining the CWT of the negative sequence component of the stator phase currents with the CNN model. CWT scalogram images are used as inputs of the CNN-based ITSC fault classifier. Experimental tests were conducted to verify the effectiveness of the proposed approach under various motor operating conditions. Moreover, the effect of the input image format, network structure, and learning process parameters on the accuracy and effectiveness of the model were investigated. The results of the experimental studies confirmed the high effectiveness and advantages of the developed method. The three main contributions and original elements of this research can be summarized as follows:

- Development of a novel hybrid method for automatic detection and classification of PMSM stator winding faults based on the combination of CWT analysis of the negative sequence component of the stator phase currents with the CNNs, which makes it possible to achieve remarkably high detection and classification effectiveness already at the initial stage of fault propagation.
- Detailed analysis of the influence of the CNN model structure, training parameters, and the input image format on the accuracy and effectiveness of the PMSM stator winding fault classifier models.
- Appropriate selection of the symptom extraction stage (CWT-based) and preparation of the input image format (compression) allowed the use of CNNs with a simple structure. This results in a short training time and a small model size, which is extremely important from the view of hardware (microcontroller) implementation of AI-based algorithms.

The article consists of seven sections. The next two sections discuss the theoretical basis of the CWT and CNNs. This is followed by a description of the laboratory stand on which the experimental tests were conducted. The next section presents the results of the extraction of PMSM stator winding fault symptoms from the signal of symmetrical components of the stator phase currents using CWT analysis. The penultimate section

discusses the automation stage of the fault diagnosis process using CNN. The whole is concluded with a summary of the research presented in the paper.

2. CONTINUOUS WAVELET TRANSFORM

Methods implementing time-frequency analysis are applied to describe the relationship between signal information in the time domain and the corresponding spectral distribution in the frequency domain [27]. CWT is one of the transforms belonging to the group of these methods. It has found application in many fields, including electric motor fault diagnosis. The result of the CWT, called a scalogram, contains both time-of-occurrence information and the distribution of harmonics in the frequency domain of the analyzed signal. The CWT of a signal $x(t)$ is defined by the following equation [28]:

$$\begin{aligned} \mathrm{CWT}(\tau,a) &= \int_{-\infty}^{\infty} x(t)\psi^*_{a,\tau}(t)\,\mathrm{d}t \\ &= \frac{1}{\sqrt{|a|}}\int_{-\infty}^{\infty} x(t)\psi^*\left(\frac{t-\tau}{a}\right)\mathrm{d}t, \end{aligned} \tag{1}$$

where: a – a scale factor, τ – a shifting parameter (in the time domain), ψ – a mother wavelet, $\psi^*(\cdot)$ – a complex conjugate of function $\psi(\cdot)$, $\psi^*_{a,\tau}$ – a scaled and translated version of ψ^*, called baby wavelet:

$$\psi^*_{a,\tau} = \frac{1}{\sqrt{|a|}}\psi^*\left(\frac{t-\tau}{a}\right). \tag{2}$$

In the actual digital implementation, the integral in equation (1) is replaced by a summation operation, according to the following equation:

$$CWT(\tau,a) = \frac{1}{\sqrt{|a|}}\sum_{n=-\infty}^{\infty} x(t)\psi^*\left(\frac{n-\tau}{a}\right). \tag{3}$$

The CWT analysis result resolution in the time and frequency domain depends on the scale factor a. This factor allows for a change in the width of the wavelet – scaling it in the time domain (changing the duration of the wavelet). It is assumed that the scale is proportional to the inverse of the frequency. In the low-frequency range of the signal, the frequency resolution is higher, and the time resolution is lower, and vice versa in the high-frequency part of the signal. This is consistent with slow changes in the low-frequency signal and fast changes in the high-frequency signal. The change in the shift factor τ corresponds o a change in the position of the wavelet in the time domain [25].

As part of the research presented in this paper, the Morse wavelet, which is available in the *MATLAB Wavelet Toolbox*, is used after an earlier comparison with other types of wavelets, such as the Bump wavelet and Morlet wavelet. The scope of the study focused on verifying the feasibility of using CWT analysis to extract the PMSM stator winding (ITSC) fault symptoms, so the theoretical description of the CWT mathematical apparatus is limited to the above basics. Nevertheless, a detailed description of the theory, properties, and implementation of these wavelets is described in [29–31].

3. CONVOLUTIONAL NEURAL NETWORKS

The past decades have seen a significant increase in popularity and progress in the field of AI. A particularly rapidly growing area of AI is deep learning (DL). The main reason for the rapid growth in popularity of DL is the high effectiveness of this technique in solving problems that cannot be optimally solved by shallow neural networks, such as the widely used multilayer perceptron (MLP).

The primary function of CNNs is to extract relevant features, including higher-order ones, from input information. The most popular application of CNNs is their use as image and speech recognition tools [32] CNNs operate on images represented as three-dimensional tensors containing two spatial axes (height and width) and a depth axis, called the channel axis. For RGB images, the depth axis is three-dimensional, while for grayscale images it is one-dimensional [33].

CNNs consist of a collection of layers of different types. The basic layers present in their structure are convolution layers (CL), pooling layers (PL), flattening layers (FL), and fully connected (dense) layers. In addition, there may also be normalization and dropout layers. Each of the subsequent convolution layers allows the extraction of characteristic features of the input image. The first layer can be understood as a filter of basic, low-order features, such as image edges or pixels with similar textures. Successive convolution layers allow the extraction of features of increasingly higher order. The depth channels of the image are processed by a set of filters. The filter output (feature map) is then subject to a nonlinear activation function [34]. In the case of CNNs, the most commonly used activation function, also applied in this study, is the rectified linear unit (ReLU) function. At the output of the convolutional layer, the number of extracted feature maps is much larger compared to the dimensionality of the input. For this reason, pooling layers are used in the CNN structure to limit the number of parameters. The flattening layers transform the resulting images, which have the form of three-dimensional tensors after the pooling operation, into a vector form that is passed to the fully connected layer.

There are many methods for training CNNs. Among the most popular is the stochastic gradient descent (SGD) algorithm. This algorithm is an optimization algorithm and is based on error estimation from a data packet containing N random samples from a data set. SGD iteratively updates the training parameters, i.e. kernels and weights. The algorithm is easy to implement and allows for online training. However, the weight updates have a large variance, and the training speed is relatively low. The variance problem can be solved by using the mini-batch SGD algorithm, while its acceleration after introducing the momentum parameter (γ). This algorithm is known by the acronym SGDM. Currently, this method is the most common choice for training CNNs, also applied within the framework of this work. The loss (objective) function used in the learning process is

sparse categorical cross-entropy (SCCE):

$$L_{\mathrm{SCCE}} = -\frac{1}{N}\sum_{i=1}^{N}\left[l_i \log(y_i) + (1-l_i)\log(1-y_i)\right], \qquad (4)$$

where N is the number of samples corresponding to the selected batch size B, l_i is the actual class, and y_i is the model response.

Among the most important parameters to be determined in the initial training phase are the learning rate η and γ. The gradient of the L_{SCCE} loss function determines the direction in which the function has the steepest rise. Each parameter (weight) w is updated in the negative direction of the gradient with a step size determined by η. The aforementioned SGDM learning method is a gradient descent acceleration technique, which accumulates a vector υ in the direction of constant decrease of the loss function. The parameter γ determines the percentage of previous gradients that are additionally taken into account when updating the weights, in addition to the current gradients. A single parameter update is implemented according to the following equations [35]:

$$\begin{aligned} \upsilon_{i+1} &= \gamma\upsilon_i - \eta\frac{\partial L_{\mathrm{SCCE}}}{\partial w_i}, \\ w_{i+1} &= w_i + \upsilon_{i+1}. \end{aligned} \qquad (5)$$

4. EXPERIMENTAL SETUP

Experimental tests were conducted on a specially prepared setup, consisting of two PMSM motors: the tested one, rated at 2.5 kW, and the second one, rated at 4.7 kW, which provided the load torque. The real view of the experimental stand is shown in Fig. 1. The parameters of the analyzed motor are grouped in Table A.1 in the Appendix. This motor was powered by a Lenze Topline 8400 frequency converter and operated in closed-loop field-oriented control (FOC) with PI current and speed controllers. The stator winding of the PMSM under test was rewound in such a way that its design allowed controlled ITSCs involving a given number of turns to be physically shorted. During the tests, a maximum of five turns were short-circuited, which corresponded to 2% of all turns in a phase. The schematic diagram of the derived phase terminals of the PMSM stator winding is shown in Fig. 2. The tests were conducted without limiting the additional resistance of the current in the shortened circuit. Diagnostic signals – stator phase currents were measured with LA 25-NP transducers by LEM. Output signals from the transducers were transferred to a data acquisition system – an eight-channel NI PXI-4492 DAQ measurement card by National Instruments (NI). The DAQ card was housed in an NI PXI 1082 industrial computer. The measurement application was prepared in the LabVIEW environment. A simplified block diagram of the test bench is shown in Fig. 3. Speed control of the test motor was implemented using Lenze Engineer software, while load level control was realized using VeriStand.

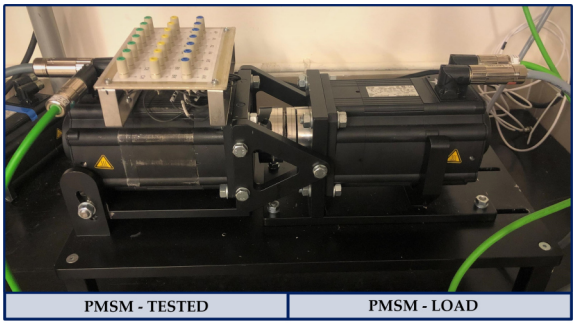

Fig. 1. Experimental stand – real view

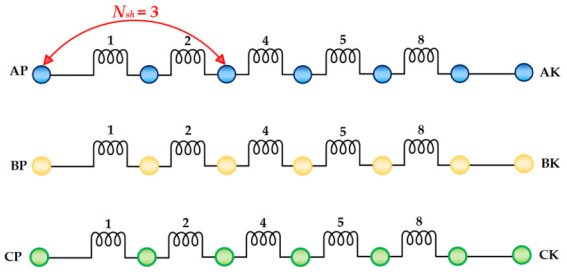

Fig. 2. Diagram of the derived phase terminals of the PMSM stator winding

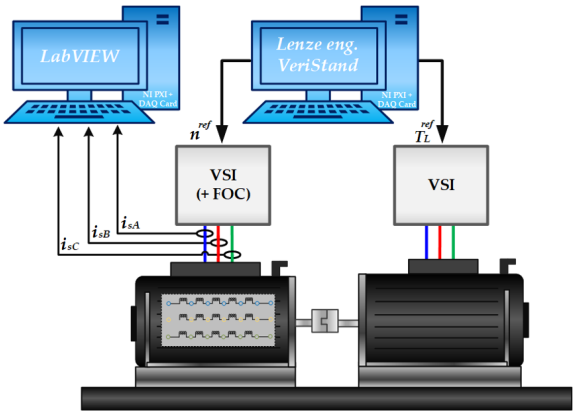

Fig. 3. Simplified block diagram of the test bench

5. PMSM STATOR WINDING FAULT SYMPTOM EXTRACTION USING CWT

The occurrence of ITSC in the PMSM winding causes an increase in the amplitude of stator currents, their fluctuation, and notable asymmetry [14]. Asymmetry occurring due to a short circuit, in turn, affects the value of the symmetrical components of the stator phase currents [36]. In this study, the possibility of extracting the symptoms of PMSM stator winding faults through CWT analysis of these components is analyzed.

The instantaneous values of stator phase current symmetrical components are calculated using a 90° phase shift operator in the time domain, according to equation (6) [32]:

$$\begin{bmatrix} i_1 \\ i_2 \end{bmatrix} = \frac{1}{3}\begin{bmatrix} i_{sA} - \frac{1}{2}(i_{sB}+i_{sC}) + \frac{\sqrt{3}}{2}S_{90}(i_{sB}-i_{sC}) \\ i_{sA} - \frac{1}{2}(i_{sB}+i_{sC}) - \frac{\sqrt{3}}{2}S_{90}(i_{sB}-i_{sC}) \end{bmatrix}, \qquad (6)$$

where i_{sA}, i_{sB}, i_{sC} – instantaneous values of the stator phase currents in the $a-b-c$ coordinate system, i_1, i_2 – instantaneous values of the positive and negative sequence components of the stator phase currents, S_{90} – 90° time domain phase shift operator.

The waveforms of the i_1 and i_2 for different levels of load torque T_L, rated supply voltage frequency $f_s = f_{sN} = 100$ Hz, and instantaneous short-circuiting of 1 to 5 turns are shown in Fig. 4. The amplitude changes of the i_1 as a result of ITSCs are evident, but the effect of the T_L level is much more visible. The percentage increase in the amplitude of i_1 caused by ITSC, especially in the incipient stage of the fault, decreases significantly at higher load. The effect of short circuits on the waveform of the i_2 is much clearer. Compared to the i_1, it can be seen that the amplitude of i_2 is less dependent on the T_L. This is a notable advantage, because in fault diagnosis, it is necessary to extract fault symptoms whose value does not depend on the operating conditions of the drive system, such as T_L and f_s, and only changes as a result of the fault. Nevertheless, the increase in amplitude at the early stage of damage – at 1 and 2 shorted turns ($N_{sh} = 1$, $N_{sh} = 2$), is small. A signal preprocessing step will be implemented to extract the symptoms of ITSCs, which are also apparent at an early stage of its development. CWT analysis will be applied to accomplish this task. CWT scalograms of the negative and positive stator phase current symmetrical component for the same PMSM operating and stator winding conditions as in the analysis of the waveforms of these components (Fig. 4) are shown in Fig. 5a and Fig. 5b, respectively.

Analyzing Fig. 5 – the i CWT scalogram, an increase in the amplitude value of the fundamental component, corresponding to the frequency of the supply voltage ($f_s = f_{sN} = 100$ Hz), can be observed as the T_L level increases. Analysis of the scalogram did not facilitate isolating the frequency components whose amplitude value increased as a result of ITSCs. Nevertheless, in the case of the i_2 CWT scalogram, a significant increase in the values of the amplitudes of the coefficients corresponding to the f_s component $|\mathrm{CWT}_{i2}(f_s,t)|$ as a result of the occurrence of a short-circuit is evident, over the entire range of the analyzed T_L and N_{sh}. It is also important that only a small effect of T_L on the value of these amplitudes is visible. CWT scalograms for rated T_L and three different f_s (rotation speeds) are shown in Fig. 6. As in the case of operation at rated f_s, in the case of the i_1 CWT result, there are no visible symptoms that could indicate PMSM stator winding fault.

Nevertheless, the value increase of the amplitudes of the fundamental harmonic f_s on the CWT scalogram of the i_2 due to the ITSC fault is visible also at reduced supply voltage frequency.

Based on the analysis of the results shown in Figs. 4–6, the results of the CWT analysis of the i_2 will be used as inputs of the fault classifier models in the process of the automatic detection and classification of the PMSM stator winding condition. The images (scalograms) resulting from CWT processing of this signal, after selecting the parts in which ITSC symptoms (covering the f_s component) are visible and properly preparing their size and color depth channels, will be used as input images. Details

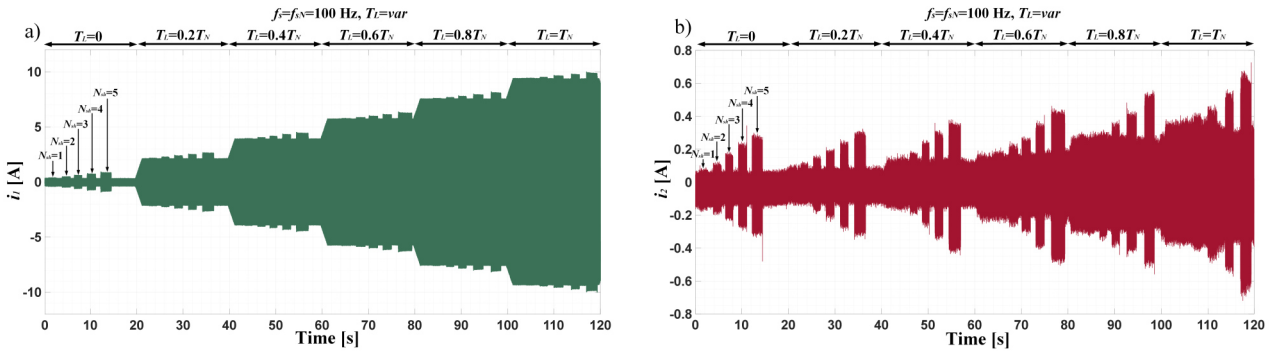

Fig. 4. The waveforms of the (a) i_1 and (b) i_2 for T_L = var, rated supply voltage frequency ($f_s = f_{sN} = 100$ Hz), and momentary short-circuiting of 1 to 5 turns in the PMSM stator winding

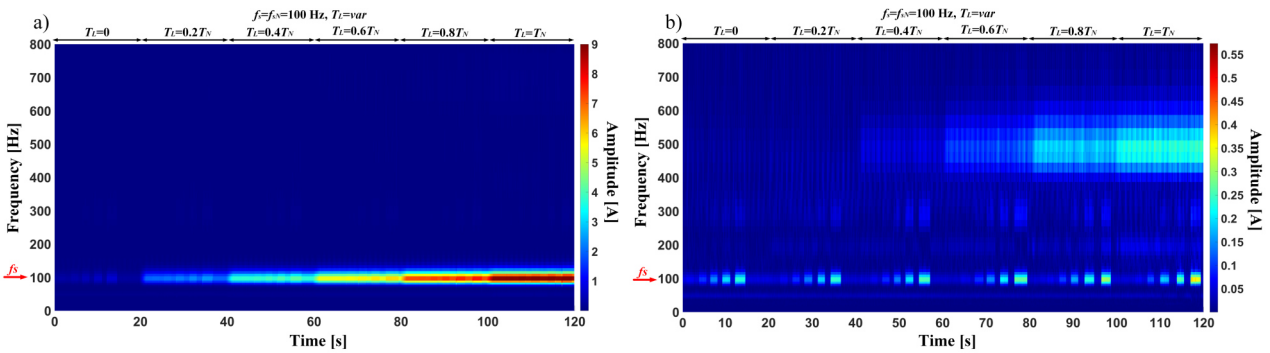

Fig. 5. CWT scalograms of the (a) i_1 and (b) i_2 for T_L = var, rated supply voltage frequency ($f_s = f_{sN} = 100$ Hz), and momentary short-circuiting of 1 to 5 turns in the PMSM stator winding

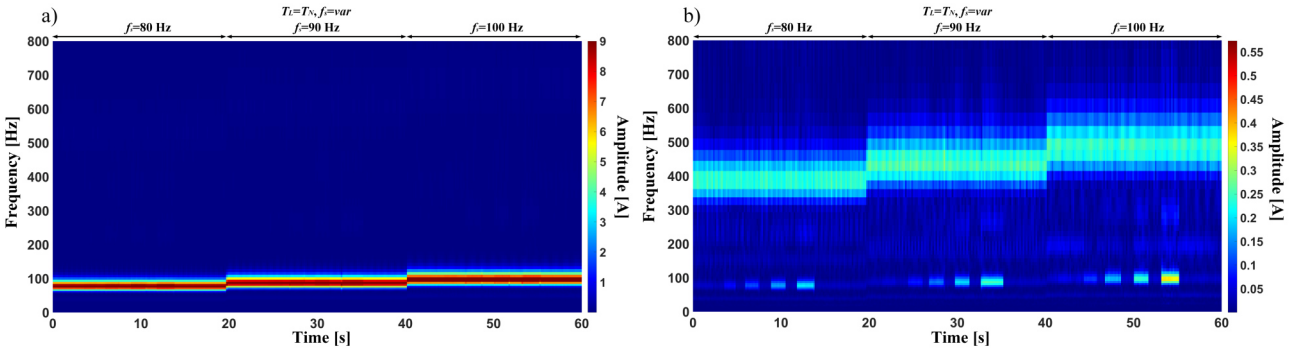

Fig. 6. CWT scalograms the (a) i_1 and (b) i_2 for f_s = var, rated load torque ($T_L = T_N$), and momentary short-circuiting of 1 to 5 turns in the PMSM stator winding

of the preparation of the images and the training and test sets will be discussed in the next sections.

6. CNN-BASED AUTOMATION OF THE PMSM STATOR WINDING FAULT DETECTION AND CLASSIFICATION

While researching fault diagnosis methods, to meet the requirements for modern diagnostic systems, in addition to the stage of fault symptom extraction, it is necessary to ensure full automation of the fault detection and classification process. The novel method proposed in this paper combines a symptom extraction step using CWT analysis with a deep neural network - CNN, which acts as a fault classifier. CNNs effectiveness in image recognition has been confirmed in research papers from many different scientific fields. To conduct the training process of the CNN model, it is necessary to prepare a dataset. The dataset, which was collected during the experimental tests, consists of 1080 images that are parts of the CWT scalogram – with the range of the frequency axis limited to 200 Hz. This range was chosen based on the analysis presented in the previous section. It covers changes that occur due to ITSC. The horizontal axis covers the range from 0 to 0.25 s, which is due to the adopted size of the data package on which the CWT analysis is implemented. This packet contains 2048 samples, which at a sampling rate of f_p = 8192 Hz corresponds to 0.25 s. The data set was randomly divided into a training set (70% – 756 images) and a test set (30% – 324 images). The images correspond to different conditions of the stator winding: $N_{sh} = \{0;\ 1;\ 2;\ 3;\ 4;\ 5\}$; load torques: $T_L = \{0;\ 0.2T_N;\ 0.4T_N;\ 0.6T_N;\ 0.8T_N;\ T_N\}$ and supply voltage frequency: $f_s = \{80\text{ Hz};\ 90\text{ Hz};\ 100\text{ Hz}\}$. Example images before compression included in the dataset for different N_{sh} and T_L are shown in Fig. 7. Nevertheless, within the scope of this work, the influence of the format of the input image on the training process and the classification effectiveness of CNN models will also be investigated. Image format (type) is meant to be the size (resolution) of the image expressed in pixels (px) and the number of color depth channels. Four types of input images were studied and compared: RGB images compressed to 32×32 and 64×64 pixels, as well as processed to grayscale (reduced from three to one color depth channels) with the same size as RGB images. Example compressed images for each of the four types tested are shown in Fig. 8.

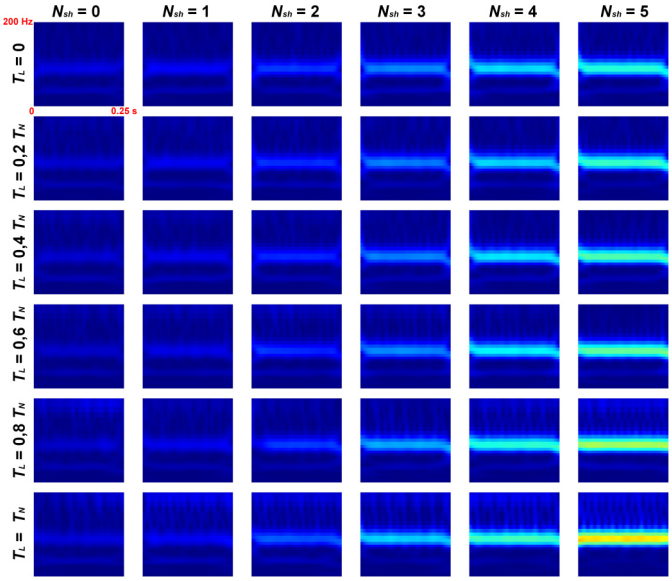

Fig. 7. Example images included in the dataset for different stator winding conditions and load torques

Based on a comparison of these images, it can be concluded that both the resolution and the number of color channels have a significant impact on the resulting image format. It can also affect the size of the model, the time of training, as well as the accuracy (precision) and effectiveness of the model, which will be further investigated.

A simplified diagram illustrating the stages of diagnostic information processing in the developed method is shown in Fig. 9. There are three main stages:

1. Measurement and acquisition of the stator phase currents, determination of the i_2, and collection of a vector (data packet), consisting of 2048 samples.
2. Signal processing of the i_2 using CWT analysis and selecting and compressing to a certain size a part of the scalogram, which is the input of the CNN model.
3. Automatic classification of the stator winding condition (N_{sh}) by the CNN model based on the input image.

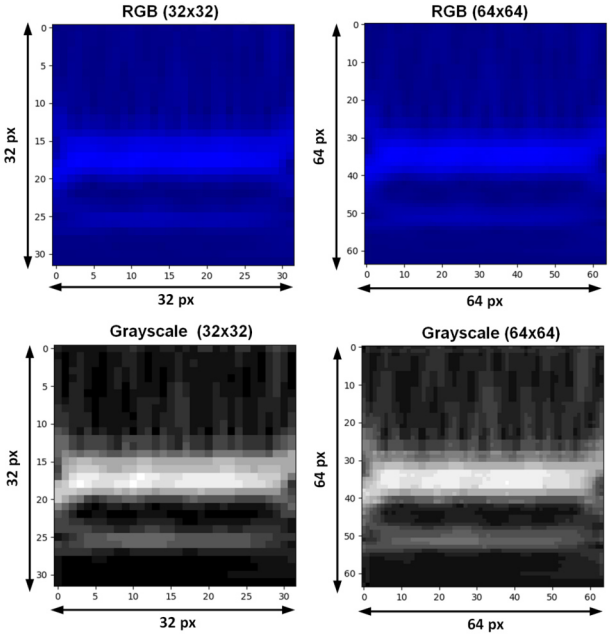

Fig. 8. Example compressed images for each of the four types of input images analyzed

The CWT analysis of the signal was implemented using the *Wavelet Toolbox* available in the MATLAB software, while the script implementing the input image preparation process, the training process and the CNN model verification were implemented in the Python language (interpreter: Python 3.9.3).

There are no clear rules for selecting the best CNN structure for a given application. Nevertheless, it directly affects the accuracy and effectiveness of the model [23,37]. This study analyzes not only the impact of CNN structure on these metrics but also the format of the input image. The key parameters and details of the structure of four of the CNN models studied (CNN-1, CNN-2, CNN-3, CNN-4) are grouped in Table 1.

Each of these structures consists of an input layer (IL) whose size corresponds to the size of the input image – $32\times32\times1$ and $64\times64\times1$ for grayscale images, and $32\times32\times3$ and $64\times64\times3$ for RGB images, CL(s), PL(s), FL layer and fully connected layer. The CNN-1 and CNN-2 models have only one convolution and pooling layer in their structure, containing 16 filters in the case of CNN-1 and 32 filters in the case of CNN-2, while CNN-3 has two convolution (32 and 64 filters) and pooling layers. The CNN-4 model has the most extensive structure and has as many as three convolution layers ($32\times64\times128$) and three pooling layers. The *ACC* (accuracy) value, also known as the precision of the CNN models, during the training process for the default training parameters ($\eta = 0.0001$, $B = 8$, $\gamma = 0.5$) for tested structures and different types of input images described earlier, is shown in Fig. 10. The model accuracy is the ratio of the number of correct classifications of the PMSM winding condition to the size of the training dataset and therefore indicates how effective the developed model is at a given stage of training. Based on the analysis of the results shown in Fig. 10, it can be concluded that in the case of the 32×32 RGB input image, in the initial stage of the training process (from 1 to about 100 epochs), the fastest matching (maximum accuracy) is achieved by the models with a more advanced structure: CNN-3 and CNN-4. At the end of the training process, the maximum accuracy ACC_{MAX}, equal to 99.87%, is achieved by the CNN-2, CNN-3, and CNN-4 models.

For the 64×64 RGB image, the highest ACC_{MAX} among the compared structures, which is as high as 100%, is achieved by the CNN-3 model. The CNN-4 model, despite its more advanced structure (three convolutional layers compared to two layers in the CNN-2 model), achieved a lower ACC_{MAX} (99.87%), which indicates that the network structure for this dataset is excessive – the over-fitting occurred. The lowest precision for both sizes of RGB images is achieved by the CNN-1 model, whose structure is the simplest. In the case of grayscale images, all the analyzed models showed a similar accuracy. Nevertheless, ACC_{MAX} is

Table 1
Key parameters of the analyzed CNN structures

<table>
<tr><th>Layer / Model</th><th>IL</th><th>Conv. 1</th><th>Pooling 1</th><th>Conv. 2</th><th>Pooling 2</th><th>Conv. 3</th><th>Pooling 3</th><th>FL</th><th>Fully connected</th></tr>
<tr><td>CNN-1</td><td rowspan="4">IL</td><td>NF: 16
FS: 3x3
AF: ReLU</td><td rowspan="4">Pooling: Max
Mask size: 2x2</td><td>Not applied</td><td>Not applied</td><td>Not applied</td><td>Not applied</td><td rowspan="4">FL</td><td rowspan="4">ON: Max
AF: Softmax
TM: SGDM</td></tr>
<tr><td>CNN-2</td><td rowspan="3">NF: 32
FS: 3x3
AF: ReLU</td><td>Not applied</td><td>Not applied</td><td>Not applied</td><td>Not applied</td></tr>
<tr><td>CNN-3</td><td rowspan="2">NF: 64
FS: 3x3
AF: ReLU</td><td rowspan="2">Pooling: Max
Mask size: 2x2</td><td>Not applied</td><td>Not applied</td></tr>
<tr><td>CNN-4</td><td>NF: 128
FS: 3x3
AF: ReLU</td><td>Pooling: Max
Mask size: 2x2</td></tr>
<tr><td colspan="10">IL – input layer, NF – number of filters, FS – filter size, AF – activation function, ON – number of output neurons, TM – training method</td></tr>
</table>

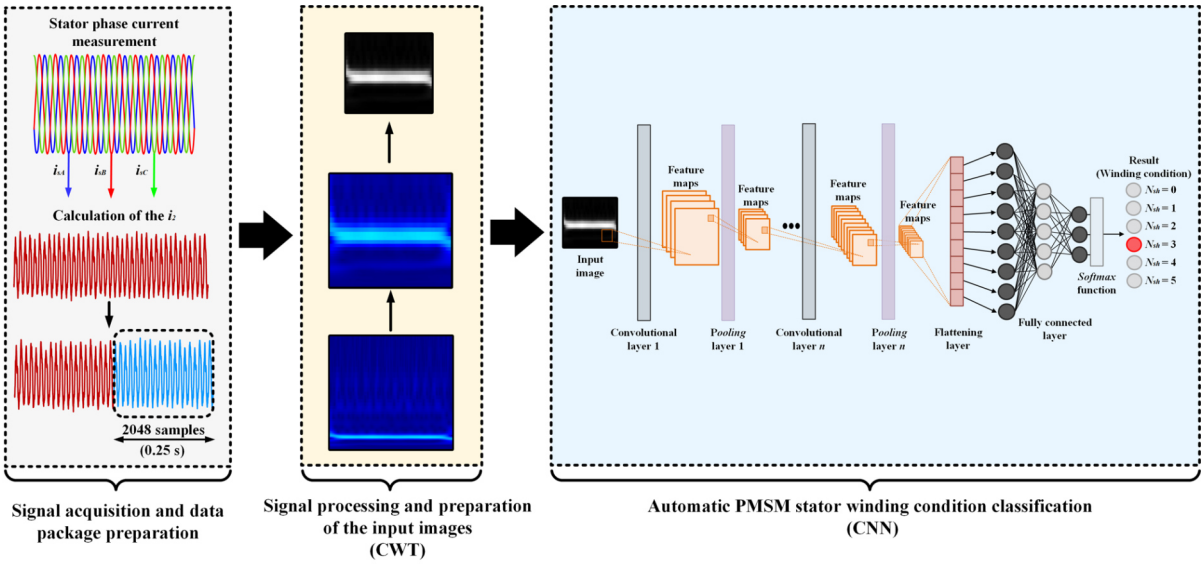

Fig. 9. Schematic diagram of the developed PMSM stator winding intelligent fault diagnosis method

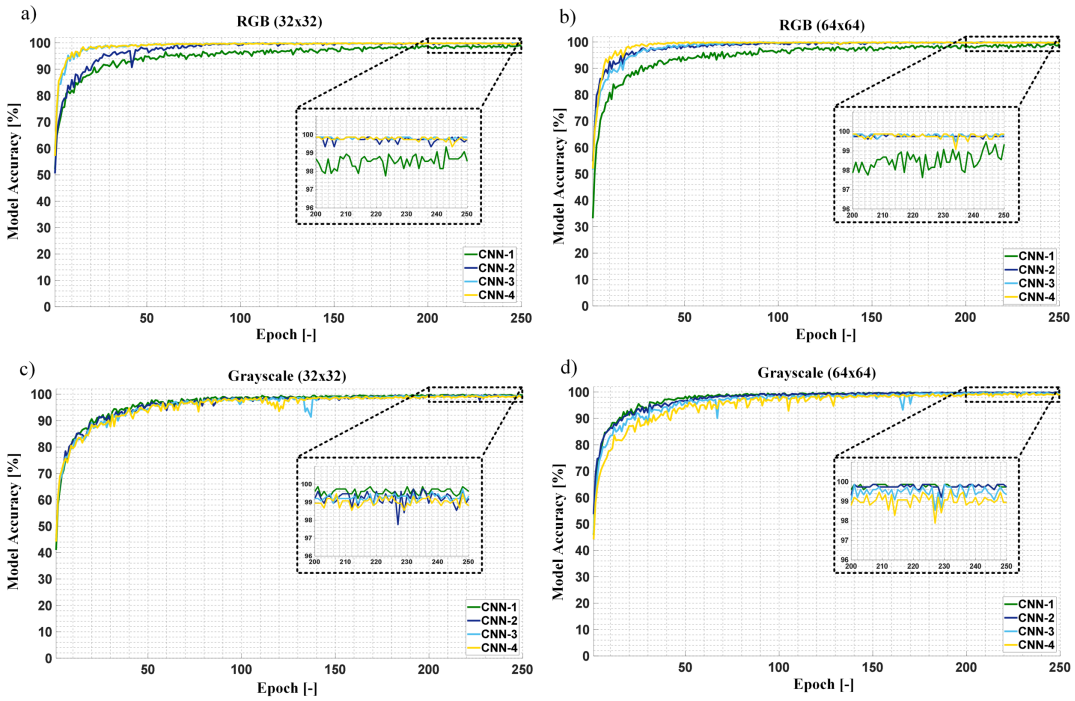

Fig. 10. CNN models accuracy during the training process for different structures and input images: (a) RGB (32×32), (b) RGB (64×64), (c) grayscale (32×32), (d) grayscale (64×64) ($\eta = 0.0001$, $B = 8$, $\gamma = 0.5$)

lower than for the RGB images - none of the models achieved $ACC_{MAX} = 100\%$. The lower accuracy is particularly evident at the initial stage of training – in the first several epochs, there is a later stabilization of precision at the maximum value. For grayscale images, the CNN-1 network achieved significantly better results than for RGB images. This is because, due to only one convolution layer with a small number of filters (16), it was not taught redundant higher-order features (patterns), irrelevant to the task (evaluation of the PMSM stator winding condition), and ultimately resulted in achieving a higher accuracy (99.87%).

To accurately analyze the course of the training process of a given CNN model for different forms of the input image, Fig. 11 shows a comparison of the accuracy of the tested models for different formats of input images. Figure 11a shows the results for the CNN-1 model. The analysis of the training process for this model confirms the previous conclusions – the highest accuracy and the fastest stabilization of the training process at the maximum value occurs for grayscale images. In the case of the CNN-2 model, the highest precision was achieved for 64×64 RGB images. Both CNN-3 and CNN-4 models, due to their more

advanced structure (two and three convolutional layers, respectively), achieved the best accuracy for RGB images. These networks, with more convolutional layers, can learn higher-order, task-relevant patterns (PMSM stator winding condition classification) that are visible in RGB images. A comprehensive comparison of ACC_{MAX}, training time (t_{train}), a minimum value of the loss function (L_{min}), and the size of individual models (M_{size}) for different input image formats are grouped in Table 2. Based on the analysis of the results, it can be concluded that the more complex the structure of the CNN, the longer the training time. In addition, the same trend can be seen for the size of the model, which is extremely important from the point of view of embedded (microcontroller) implementation, where memory is significantly limited, and it is necessary to use optimized solutions. Comparing the size of the CNN-2 and CNN-3 models, it was found that the use of an additional pooling layer (CNN-3) results in a reduction of parameters and, consequently, network size. A comparison of training time for different input image formats and CNN model structures is shown in Fig. 12. From this comparison, it can be seen that in addition to the structure size, the longer training time is also significantly affected by image size (resolution). For 64×64 images, the training time is significantly longer than for 32×32 images. Summarizing the comparative analysis of the models, each model achieved a high accuracy of more than 99.0%. The CNN-3 model has the highest precision (100.0%). However, due to its more advanced structure, the training time is longer compared to the CNN-1 and CNN-2 models.

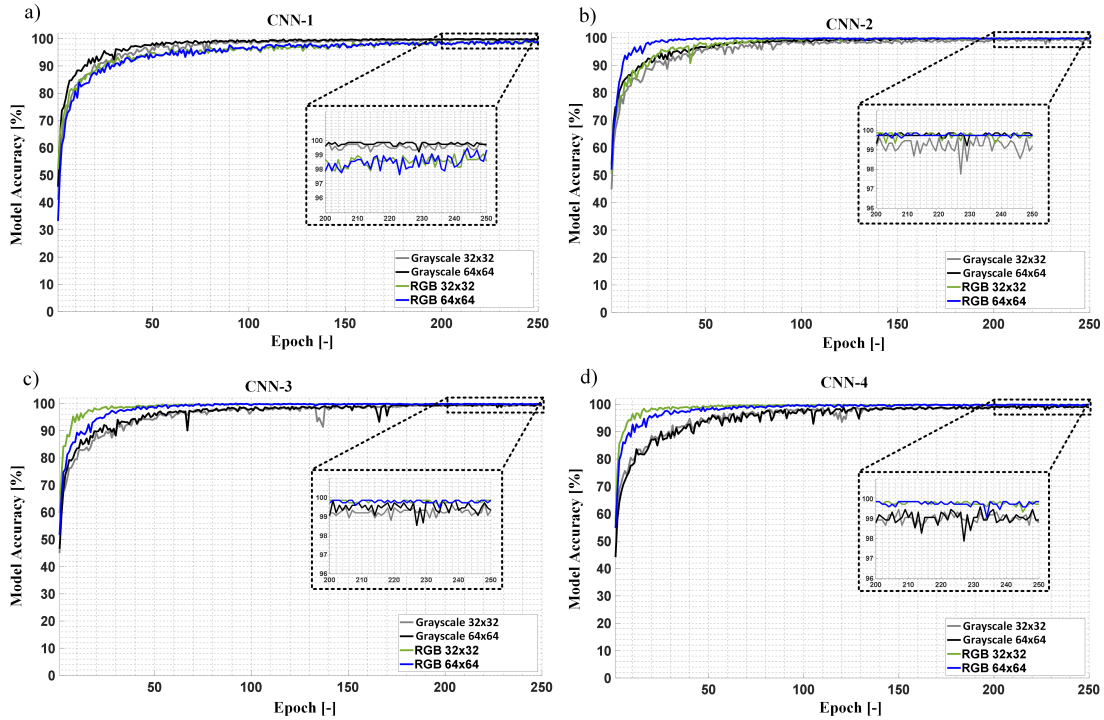

Fig. 11. CNN models accuracy during the training process for different input images and network structures: (a) CNN-1, (b) CNN-2, (c) CNN-3, (d) CNN-4 ($\eta = 0.0001$, $B = 8$, $\gamma = 0.5$)

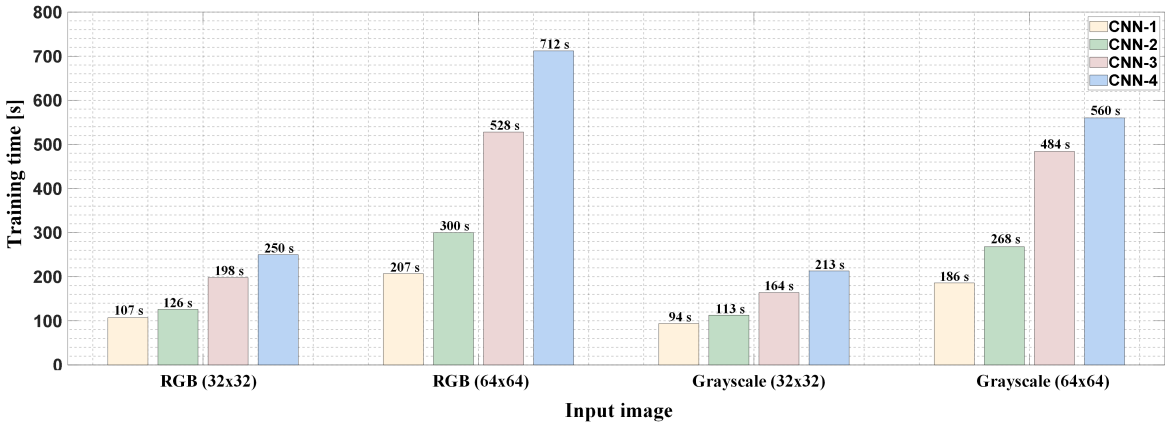

Fig. 12. Comparison of training time for the tested CNN models and different formats of input images

Table 2
Comparison of accuracy, size and training time for different CNN model structures and input image formats

Image / Model	RGB (32x32)				RGB (64x64)				Grayscale (32x32)				Grayscale (64x64)			
	ACC_{MAX}	L_{min}	M_{size}	t_{train}	ACC_{MAX}	L_{min}	M_{size}	t_{train}	ACC_{MAX}	L_{min}	M_{size}	t_{train}	ACC_{MAX}	L_{min}	M_{size}	t_{train}
CNN-1	99.34%	0.0439	98 kB	107 s	99.47%	0.0333	385 kB	207 s	99.87%	0.0252	97 kB	94 s	99.87%	0.0147	384 kB	186 s
CNN-2	99.87%	0.0063	196 kB	126 s	99.87%	0.0058	772 kB	300 s	99.74%	0.0272	193 kB	113 s	99.87%	0.0173	769 kB	268 s
CNN-3	99.87%	0.0075	172 kB	198 s	100.00%	0.0039	460 kB	528 s	99.74%	0.0333	170 kB	164 s	99.87%	0.0200	458 kB	484 s
CNN-4	99.87%	0.0069	412 kB	250 s	99.87%	0.0081	557 kB	712 s	99.48%	0.0379	410 kB	213 s	99.60%	0.0278	554 kB	560 s

ACC_{MAX} - maximum model accuracy, L_{min} - minimum loss function value, M_{size} - model size, t_{train} - training time

The above comparison and evaluation of model accuracy for different structures and forms of input images are not sufficient, because, despite the high precision of the model, it may have insufficient generalization capabilities and not provide correct responses for new, unknown data. For this reason, the effectiveness of the models for the images that are in the test set is analyzed. The confusion matrices for the responses of the analyzed models for this set, different input image formats, and network structures are shown in Fig. 13.

Comparisons of classification effectiveness (the ratio of correct model responses to the size of the test set) are grouped in Table 3. For the CNN-1 model, numerous misclassifications are

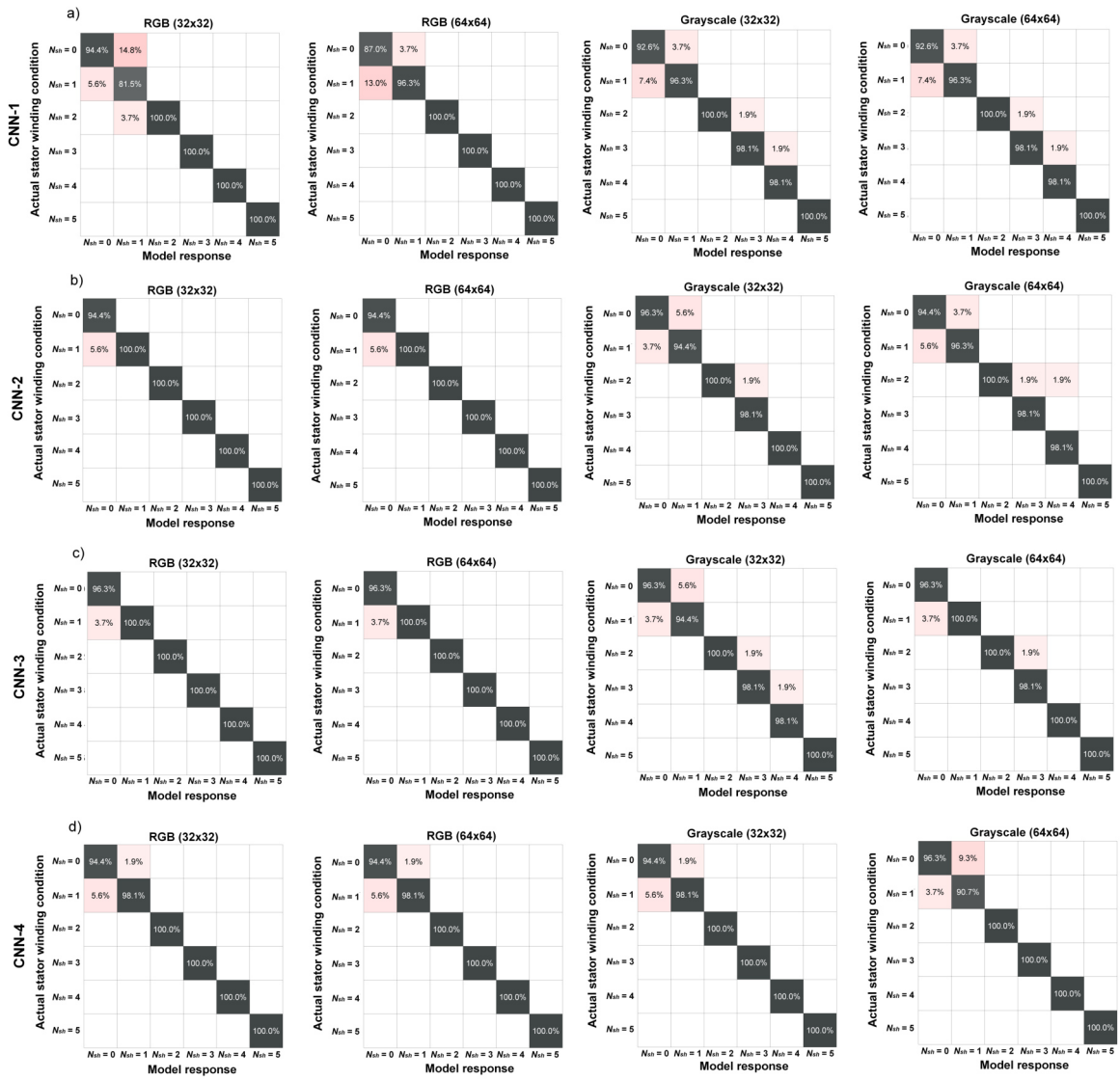

Fig. 13. Comparison of training time for the tested CNN models and different forms of input image

Table 3
Comparison of PMSM stator winding condition classification effectiveness for different models and input image formats

Image / Model	RGB (32x32)	RGB (64x64)	Grayscale (32x32)	Grayscale (64x64)
	Classification effectiveness	Classification effectiveness	Classification effectiveness	Classification effectiveness
CNN-1	95.99%	97.22%	97.53%	97.53%
CNN-2	99.07%	99.07%	98.15%	97.84%
CNN-3	99.38%	99.38%	97.84%	99.07%
CNN-4	98,.77%	98.77%	97.84%	97.84%

evident between undamaged winding ($N_{sh} = 0$) and one shorted turn ($N_{sh} = 1$) for all four input image forms analyzed. For this model, fewer misclassifications (efficiency equal to 97.53%) occur for the grayscale images, confirming previous conclusions. The CNN-2, CNN-3 and CNN-4 models achieved the highest effectiveness for RGB images, which also confirms that some higher-order features characteristic of ITSC are not visible in grayscale images.

The highest effectiveness, equal to 99.38%, is achieved by the CNN-3 model, with a structure containing two CLs and two PLs. The CNN-4 model, despite three CLs, achieved a lower efficiency (98.87%), which may be indicative of a too-advanced structure and learning patterns that are not relevant to PMSM winding condition classification and result in erroneous responses.

It should be noted that each of the developed models achieved high classification efficiency, which confirms the validity of using CWT of the negative sequence stator phase currents component to extract ITSC symptoms in the PMSM stator winding and the high effectiveness of the developed method.

In addition to the structure of the CNN model and the form of the input image, the training process can also be influenced by key training parameters, which were comprehensively studied and confirmed in [37]. The analysis of the possibility of increasing the accuracy and classification effectiveness of the model was conducted for the CNN-3 structure, which has a relatively simple structure (two CLs) and achieved the best results in the comparative analysis presented before.

The effect of the value of the learning rate η on model accuracy is shown in Fig. 14a. Based on this comparison, it can

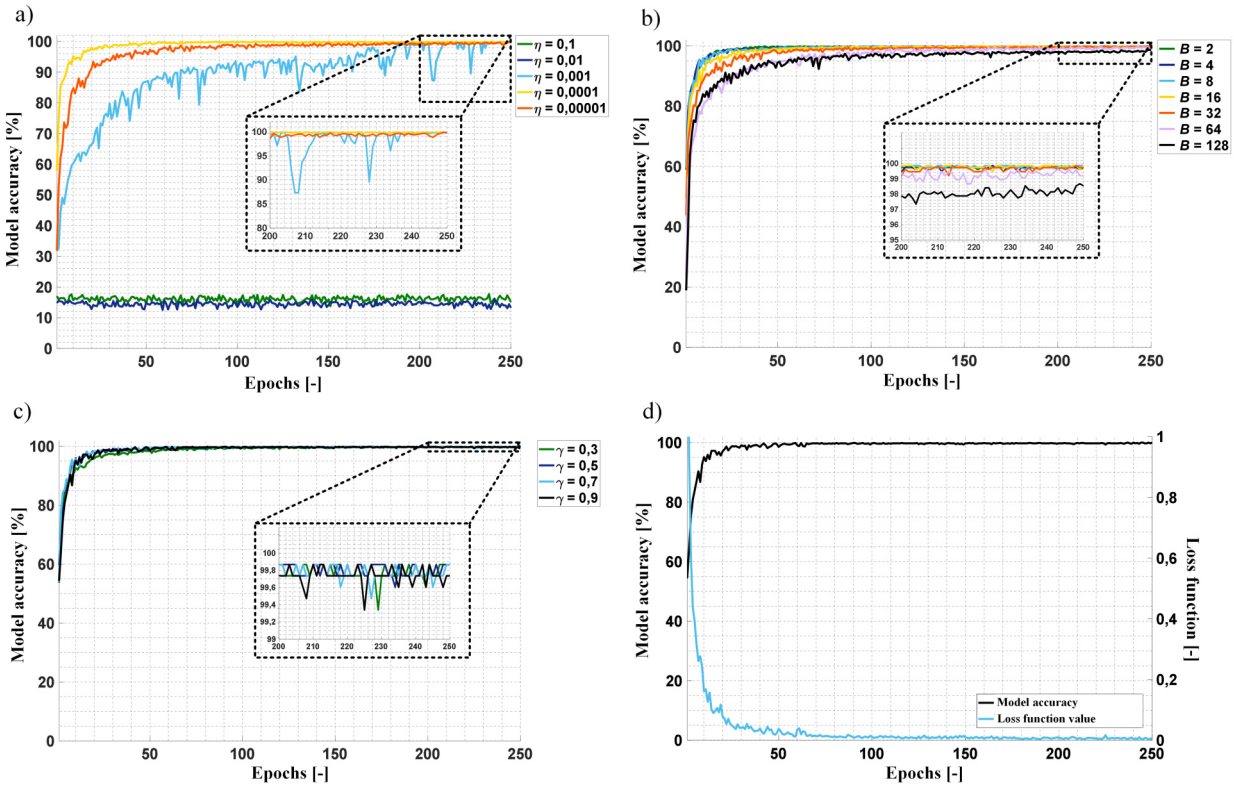

Fig. 14. CNN models accuracy during the training process for different input images and network structures: (a) CNN-1, (b) CNN-2, (c) CNN-3, (d) CNN-4 ($\eta = 0.0001$, $B = 8$, $\gamma = 0.5$)

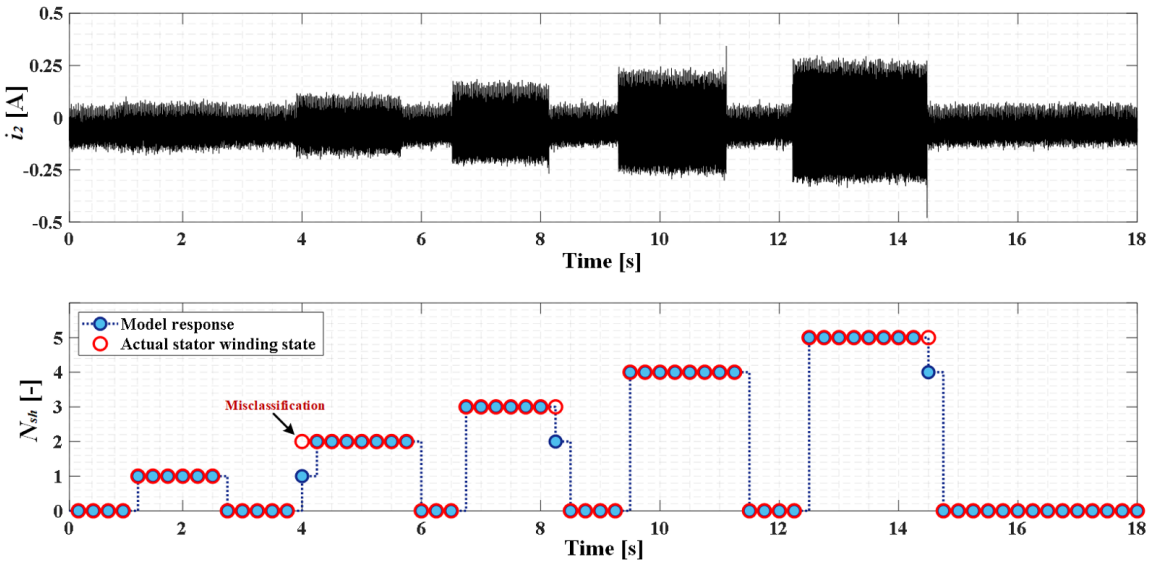

Fig. 15. The (a) i_2 waveform and (b) CNN model responses for the test during the online operation of the drive system

be concluded that if the value of η is too high, there is a stuck in the local minimum of the loss function, and consequently the model accuracy is low because the loss function does not reach the global minimum. For lower values of the learning rate, the maximum model accuracy oscillates around a similar value (100%), but the time to reach the maximum value is longer – the training process is less dynamic. The best CNN performance was obtained for $\eta = 0.0001$ which was also the default value when comparing models at an earlier stage of this study. As it can be seen, for $\eta = 0.001$ the training process was less stable, and a large variance and slower convergence to the maximum value are evident.

During the CNN training process, it is not possible to simultaneously train the model from all the samples in the dataset. This is due, among others, to the limited memory size of the central processing unit (CPU) or graphics processing unit (GPU). For this reason, the training dataset is divided into packets (batches) of a given dimension – B. The accuracy of the CNN model for different values of B is shown in Fig. 14b. Based on the analysis of the results shown in this figure, it can be seen that too high B causes the accuracy value to settle on a maximum value much later. Moreover, the maximum model precision is lower than in the case of $B \leq 16$. Nevertheless, the lower the value of B, the longer the training process. The best compromise is $B = 8$. In the last step, the effect of the γ factor on the CNN accuracy was verified. The slowest stabilization of the model accuracy occurred for $\gamma = 0.3$. For the other γ analyzed, the results were similar. The model accuracy and the value of the loss function for CNN-3 after tuning the training parameters ($\eta = 0.0001$, $B = 8$, $\gamma = 0.9$) are shown in Fig. 14d.

By tuning the training parameters, the classification effectiveness (the response to images being in the test set) slightly increased from 99.38% to 99.69%.

In the final stage of the research, the developed method was verified during the online operation of the drive system. During this test, one to five turns were momentarily short-circuited sequentially for different load torque – from 0 to the rated value T_N with a step of $0.2T_N$. An example from the verification for a motor running without a load is shown in Fig. 15. Figure 15a shows the i_2 waveform and Fig. 15b shows the CNN model response and the actual winding condition. Based on the analysis of the actual winding condition and the model response, its high precision can be observed. The achieved model detection efficiency is equal to 99.38%, while the classification efficiency equals 97.5%.

In the ITSC fault detection and classification, the detection time is especially important. The time needed to generate information about the current PMSM stator winding condition consists of measurement (stator phase current signal data collection) time, signal processing (CWT) time, input image export time, and CNN model response time. The data collection time is set to 250 ms. The times required to realize each of the remaining steps of the developed method are presented in Fig. 16. The average time for 300 trials of the CWT analysis, the export of the input image, and the CNN model response are equal to 3 ms, 23 ms, and 54 ms, respectively. It gives 80 ms on average in total. Adding the data collection time, the longest time required to detect the PMSM stator winding fault is equal to 330 ms.

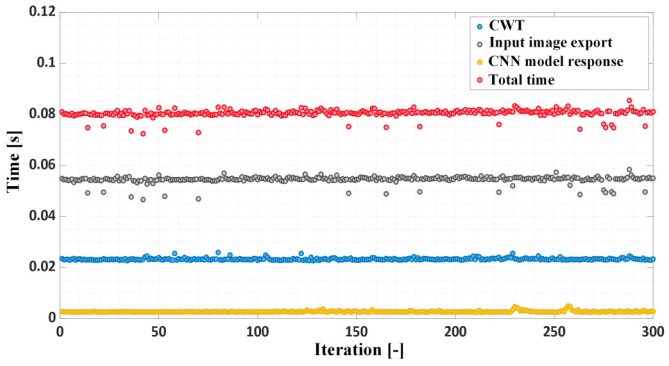

Fig. 16. The times required to realize each step of the developed method

7. CONCLUSIONS

This paper proposes and verifies experimentally a novel hybrid method for automatic PMSM stator winding fault detection and classification, which is based on the combination of CWT of the negative sequence component of the stator phase currents and CNN model. Compressed images - parts of the CWT analysis result (scalogram) were used as input values of the CNN model, which allowed full automation of the process of inferring the winding condition, achieving extremely high effectiveness. Compared to the use of classical machine learning algorithms and shallow neural networks, such as MLP, in combination with STFT or CWT [38], the developed solution made it possible to achieve a fault classification efficiency higher by about 2% (97.5%), despite the lack of the need to include in the input vector the information on load torque or supply voltage frequency. Moreover, due to the use of signal and image preprocessing as input to the CNN model, the training time achieved is several times less than when based on the raw current signal. These are the undoubted advantages of the developed solution.

Based on the analysis of experimental studies, it can be concluded that it is a solution that has a remarkably high effectiveness of winding classification already at an incipient stage of the fault propagation - with only one shorted turn, so it can be perfectly suitable as a module of diagnostic systems in modern drive systems.

According to the literature review and the authors' best knowledge, this research seems to be the first paper to propose a combination of CWT of the negative sequence stator phase current component with CNN for fault diagnosis of PMSM stator windings. In addition to the influence of the structure and training parameters, this paper analyzes in detail the influence of the form of the input image on the accuracy and effectiveness of the models, which is another original contribution. Compared to the CNN structures described in the literature used in fault diagnosis of AC motors, the proposed structure, thanks to the use of an appropriately selected symptom extraction stage and preparation of the input image format, allows the use of networks with a much less complex structure (only two convolutional and pooling layers). This results not only in the aforementioned shorter training time but also in a smaller model size, which is extremely important from the point of view of hardware implementation of artificial intelligence-based algorithms.

To apply the developed fault diagnostic method in a real drive system during online operation, it is necessary to have access to the measurement of three motor phase currents, which should be used to calculate their negative sequence component, and then process this signal using CWT analysis. Images of the scalogram (CWT result) should be used to train a CNN model developed using the Python programming language and the *Keras* open-source library. The computerized fault diagnosis system developed based on the proposed method will allow real-time monitoring of the condition of the PMSM stator winding. Further research will focus on the implementation of the proposed method in such a fault diagnostic system and the extension of functionality to include localization of the faulty phase, including in transients.

Further work will also focus on analyzing the possibility of hardware implementation (using a low-cost microcontroller) of solutions based on deep learning.

APPENDIX

Table A.1
Rated parameters of the tested PMSM

Parameter	Symbol	Value
Power	P_N	2500 W
Torque	T_N	16 Nm
Rotation speed	n_N	1500 rpm
Stator phase voltage	U_{sN}	325 V
Stator phase current	I_{sN}	6.6 A
Frequency	f_{sN}	100 Hz
Pole pairs number	p_p	4
Number of turns in one phase	N_s	2×125

REFERENCES

[1] T. Peng, C. Ye, C. Yang, Z. Chen, K. Liang, and X. Fan, "A novel fault diagnosis method for early faults of PMSMs under multiple operating conditions", *ISA Trans.*, vol. 130, pp. 463–476, Nov. 2022, doi: 10.1016/j.isatra.2022.04.023.

[2] X. Zhou, J. Sun, P. Cui, Y. Lu, M. Lu, and Y. Yu, "A Fast and Robust Open-Switch Fault Diagnosis Method for Variable-Speed PMSM System", *IEEE Trans Power Electron*, vol. 36, no. 3, pp. 2598–2610, 2021, doi: 10.1109/TPEL.2020.3013628.

[3] S. Huang, A. Aggarwal, E.G.Strangas, K. Li, F. Niu, and X. Huang, "Robust Stator Winding Fault Detection in PMSMs With Respect to Current Controller Bandwidth", *IEEE Trans. Power Electron.*, vol. 36, no. 5, pp. 5032–5042, 2021, doi: 10.1109/TPEL.2020.3030036.

[4] K.H.Baruti, C. Li, F. Erturk, and B. Akin, "Online Stator Inter-Turn Short Circuit Estimation and Fault Management in Permanent Magnet Motors", *IEEE Trans. Energy Convers.*, vol. 38, no. 2, pp. 1016–1027, 2023, doi: 10.1109/TEC.2022.3220544.

[5] P. Pietrzak and M. Wolkiewicz, "Stator winding fault detection of permanent magnet synchronous motors based on the bispectrum analysis", *Bull. Pol. Acad. Sci. Tech. Sci.*, vol. 7, no. 2, p. e140556, 2022, doi: 10.24425/bpasts.2022.140556.

[6] L. Liu, K. Wang, L.L.Guo, and J. Li, "Analysis of Inter-Turn Short Circuit Faults in Dual Three-Phase PMSM for Electromechanical Actuator", *EEE Trans. Transp. Electrif.*, vol. 9, no. 3, pp. 4059–4070, Sep. 2023, doi: 10.1109/TTE.2023.3239632.

[7] G. Niu, X. Dong, and Y. Chen, "Motor Fault Diagnostics Based on Current Signatures: A Review", *IEEE Trans. Instrum. Meas.*, vol. 72, pp. 1–19, 2023, doi: 10.1109/TIM.2023.3285999.

[8] T. Orlowska-Kowalska *et al.,* "Fault Diagnosis and Fault-Tolerant Control of PMSM Drives–State of the Art and Future Challenges", *IEEE Access*, vol. 10, pp. 59979–60024, 2022, doi: 10.1109/ACCESS.2022.3180153.

[9] Y. Chen, S. Liang, W. Li, H. Liang, and C. Wang, "Faults and Diagnosis Methods of Permanent Magnet Synchronous Motors: A Review", *Appl. Sci.*, vol. 9, no. 10, p.‘2116, 2019, doi: 10.3390/app9102116.

[10] Z. Dogan and K. Tetik, "Diagnosis of Inter-Turn Faults Based on Fault Harmonic Component Tracking in LSPMSMs Working Under Nonstationary Conditions", *IEEE Access*, vol. 9, pp. 92101–92112, 2021, doi: 10.1109/ACCESS.2021.3092605.

[11] M. Skowron, "Application of deep learning neural networks for the diagnosis of electrical damage to the induction motor using the axial flux", *Bull. Pol. Acad. Sci. Tech. Sci.*, vol. 68, no. 5, pp. 1031–1038, 2020, doi: 10.24425/bpasts.2020.134664.

[12] P. Ewert, T. Orlowska-Kowalska, and K. Jankowska, "Effectiveness Analysis of PMSM Motor Rolling Bearing Fault Detectors Based on Vibration Analysis and Shallow Neural Networks", *Energies*, vol. 14, no. 3, p. 712, 2021, doi: 10.3390/en14030712.

[13] M. Krzysztofiak, T. Zawilak, and G. Tarchała, "Online control signal-based diagnosis of interturn short circuits of PMSM drive", *Arch. Electr. Eng.*, vol. 72, no. 1, pp. 103–124, 2023, doi: 10.24425/aee.2023.143692.

[14] P. Pietrzak and M. Wolkiewicz, "Comparison of Selected Methods for the Stator Winding Condition Monitoring of a PMSM Using the Stator Phase Currents", *Energies*, vol. 14, no. 6, p. 1630, 2021, doi: 10.3390/en14061630.

[15] P. Pietrzak, M. Wolkiewicz, and T. Orlowska-Kowalska, "PMSM Stator Winding Fault Detection and Classification Based on Bispectrum Analysis and Convolutional Neural Network", *IEEE Trans. Ind.l Electron.*, vol. 70, no. 5, pp. 5192–5202, 2023, doi: 10.1109/TIE.2022.3189076.

[16] J. Urresty, J. Riba, L. Romeral, J. Rosero, and J. Serna, "Stator short circuits detection in PMSM by means of Hilbert-Huang transform and energy calculation", in *2009 IEEE International Symposium on Diagnostics for Electric Machines, Power Electronics and Drives*, IEEE, 2009, pp. 1–7, doi: 10.1109/DEMPED.2009.5292789.

[17] P. Pietrzak and M. Wolkiewicz, "Stator Phase Current STFT analysis for the PMSM Stator Winding Fault Diagnosis", in *2022 International Symposium on Power Electronics, Electrical Drives, Automation and Motion (SPEEDAM)*, IEEE, 2022, pp. 808–813. doi: 10.1109/SPEEDAM53979.2022.9841990.

[18] P. Pietrzak and M. Wolkiewicz, "Condition Monitoring and Fault Diagnosis of Permanent Magnet Synchronous Motor Stator Winding Using the Continuous Wavelet Transform and Machine Learning", *Power Electron. Drives*, vol. 9, no. 1, pp. 106–121, Jan. 2024, doi: 10.2478/pead-2024-0007.

[19] G.R.Agah, A. Rahideh, H. Khodadadzadeh, S.M. Khoshnazar, and S. Hedayati Kia, "Broken Rotor Bar and Rotor Eccentricity Fault Detection in Induction Motors Using a Combination of Discrete Wavelet Transform and TeagerKaiser Energy Operator", *IEEE Trans. Energy Convers.*, vol. 37, no. 3, pp. 2199–2206, 2022, doi: 10.1109/TEC.2022.3162394.

[20] K.-J. Shih, M.-F. Hsieh, B.-J. Chen, and S.-F. Huang, "Machine Learning for Inter-Turn Short-Circuit Fault Diagnosis in Permanent Magnet Synchronous Motors", *IEEE Trans. Magn.*, vol. 58, no. 8, pp. 1–7, Aug. 2022, doi: 10.1109/TMAG.2022.3169173.

[21] M. Skowron, T. Orlowska-Kowalska, and C.T.Kowalski, "Diagnosis of Stator Winding and Permanent Magnet Faults of PMSM Drive Using Shallow Neural Networks", *Electronics*, vol. 12, no. 5, p. 1068, 2023, doi: 10.3390/electronics12051068.

[22] M. Skowron, T. Orlowska-Kowalska, and C.T. Kowalski, "Detection of Permanent Magnet Damage of PMSM Drive Based on Direct Analysis of the Stator Phase Currents Using Convolutional Neural Network", *IEEE Trans. Ind. Electron.,*, vol. 69, no. 12, pp. 13665–13675, 2022, doi: 10.1109/TIE.2022.3146557.

[23] S. Shao, R. Yan, Y. Lu, P. Wang, and R.X.Gao, "DCNN-Based Multi-Signal Induction Motor Fault Diagnosis", *IEEE Trans Instrum. Meas.*, vol. 69, no. 6, pp. 2658–2669, 2020, doi: 10.1109/TIM.2019.2925247.

[24] Z. Li *et al.,* "Data-Driven Diagnosis of PMSM Drive with Self-Sensing Signal Visualization and Deep Transfer Learning", *IEEE Trans. Energy Convers.*, pp. 1–12, 2024, doi: 10.1109/TEC.2023.3331580.

[25] M. Skowron, "Development of a universal diagnostic system for stator winding faults of induction motor and PMSM based on transfer learning", in *2023 IEEE 14th International Symposium on Diagnostics for Electrical Machines, Power Electronics and Drives (SDEMPED)*, IEEE, Aug. 2023, pp. 517–523, doi: 10.1109/SDEMPED54949.2023.10271444.

[26] M. Skowron, M. Krzysztofiak, and T. Orlowska-Kowalska, "Effectiveness of Neural Fault Detectors of Permanent Magnet Synchronous Motor Trained With Symptoms From Field-Circuit Modeling", *IEEE Access*, vol. 10, pp. 104598–104611, 2022, doi: 10.1109/ACCESS.2022.3211087.

[27] L. Cohen, "Time-frequency distributions-a review", *Proc. IEEE*, vol. 77, no. 7, pp. 941–981, 1989, doi: 10.1109/5.30749.

[28] N. Diao, Z. Wang, H. Ma, and W. Yang, "Fault Diagnosis of Rolling Bearing Under Variable Working Conditions Based on CWT and T-ResNet", *J. Vibr. Eng. Technol.*, vol. 11, pp. 3747–3757, 2022, doi: 10.1007/s42417-022-00780-w.

[29] J.M.Lilly and S.C.Olhede, "Higher-Order Properties of Analytic Wavelets", *IEEE Trans. Signal Process.*, vol. 57, no. 1, pp. 146–160, 2009, doi: 10.1109/TSP.2008.2007607.

[30] J.M. Lilly and S.C. Olhede, "On the Analytic Wavelet Transform", *IEEE Trans. Inf. Theory*, vol. 56, no. 8, pp. 4135–4156, Aug. 2010, doi: 10.1109/TIT.2010.2050935.

[31] J.M. Lilly and S.C. Olhede, "Generalized Morse Wavelets as a Superfamily of Analytic Wavelets", *IEEE Trans. Signal Process.*, vol. 60, no. 11, pp. 6036–6041, 2012, doi: 10.1109/TSP.2012.2210890.

[32] S. Osowski, "Deep neural networks in application to data mining", *Przegląd Telekomunikacyjny i Wiadomości Telekomunikacyjne*, vol. 5, pp. 112–121, 2018.

[33] F. Chollet, *Deep learning with Python*. New York: Manning Publications, 2017.

[34] S. Lawrence, C.L.Giles, Ah Chung Tsoi, and A.D.Back, "Face recognition: a convolutional neural-network approach", *IEEE Trans. Neural Netw.*, vol. 8, no. 1, pp. 98–113, 1997, doi: 10.1109/72.554195.

[35] I. Sutskever, J. Martens, G. Dahl, and G. Hinton, "On the importance of initialization and momentum in deep learning", in *Proc. 30th International Conference on Machine Learning*, USA: PMLR, 2013, vol. 28, pp. 1139–1147.

[36] P. Pietrzak and M. Wolkiewicz, "On-line Detection and Classification of PMSM Stator Winding Faults Based on Stator Current Symmetrical Components Analysis and the KNN Algorithm", *Electronics*, vol. 10, no. 15, p. 1786, 2021, doi: 10.3390/electronics10151786.

[37] M. Skowron, C.T.Kowalski, and T. Orlowska-Kowalska, "Impact of the Convolutional Neural Network Structure and Training Parameters on the Effectiveness of the Diagnostic Systems of Modern AC Motor Drives", *Energies*, vol. 15, no. 19, p. 7008, 2022, doi: 10.3390/en15197008.

[38] P. Pietrzak and M. Wolkiewicz, "Fault Diagnosis of PMSM Stator Winding Based on Continuous Wavelet Transform Analysis of Stator Phase Current Signal and Selected Artificial Intelligence Techniques", *Electronics*, vol. 12, no. 7, p. 1543, 2023, doi: 10.3390/electronics12071543.